European Journal of Medicinal Chemistry 243 (2022) 114792

Contents lists available at ScienceDirect

European Journal of Medicinal Chemistry

journal homepage: www.elsevier.com/locate/ejmech

Research paper

Modulation of FLT3-ITD and CDK9 in acute myeloid leukaemia cells by novel proteolysis targeting chimera (PROTAC)

Eva Řezníčková [a,1], Soňa Krajčovičová [b,1], Miroslav Peřina [a], Markéta Kovalová [a], Miroslav Soural [b,**], Vladimír Kryštof [a,c,*]

[a] Department of Experimental Biology, Faculty of Science, Palacký University Olomouc, Šlechtitelů 27, 78371, Olomouc, Czech Republic
[b] Department of Organic Chemistry, Faculty of Science, Palacký University Olomouc, 17. Listopadu 12, 77146, Olomouc, Czech Republic
[c] Institute of Molecular and Translational Medicine, Faculty of Medicine and Dentistry, Palacký University Olomouc, Hněvotínská 5, 77900, Olomouc, Czech Republic

ARTICLE INFO

Keywords:
Acute myeloid leukaemia
FLT3
CDK9
Proteolysis targeting chimera (PROTAC)

ABSTRACT

Oncogenic mutations in gene encoding FLT3 kinase are often detected in acute myeloid leukaemia (AML) patients, and several potent kinase inhibitors have been developed. However, the FLT3 inhibitor treatment often leads to the resistance development and subsequent relapse. Targeted degradation of oncogenic protein kinases has emerged as a feasible pharmacological strategy, providing more robust effect over traditional competitive inhibitors. Based on previously developed competitive inhibitor of FLT3 and CDK9, we have designed and prepared a novel pomalidomide-based PROTAC. A series of biochemical and cellular experiments showed selectivity towards FLT3-ITD bearing AML cells and confirmed proteasome-dependent mechanism of action. Dual FLT3-ITD and CDK9 protein degradation resulted in the block of FLT3-ITD downstream signalling pathways, apoptosis activation and cell cycle arrest of FLT3-ITD AML cells. Moreover, transcriptional repression caused by CDK9 degradation significantly reduced expression of crucial genes involved in AML pathogenesis. The obtained results indicate the beneficial impact of simultaneous FLT3-ITD/CDK9 degradation for AML therapy.

1. Introduction

Acute myeloid leukaemia (AML) is a haematological malignant disease characterized by high numbers of abnormally differentiated immature myeloid cells infiltrated in the blood, bone marrow and other tissues [1]. It is the most frequent type of acute leukaemia in adults, causing 62% of all leukaemia related deaths [2]. Evaluating the genetic background of AML patients revealed that several frequently mutated genes play a crucial role in the disease's development [1], including FMS-like tyrosine kinase 3 (FLT3, CD135). FLT3 is one of the 56 human receptor tyrosine kinases (RTKs), and its expression is almost exclusively bound to haematopoietic stem and progenitor cells, where it is involved in the regulation of their proper maturation and function in normal haematopoiesis. Activating mutations in the FLT3 gene can be detected in one-third of AML patients ranking them among the most common drivers of the disease [3]. Internal tandem duplications (ITDs) in the juxtamembrane domain, as well as point mutations in the tyrosine kinase domain (TKD), disrupt FLT3 autoinhibitory function and allow clonal expansion of immature blood progenitors [3]. As these findings revealed FLT3 plays a crucial role in AML pathology, the extensive research into the field of FLT3 inhibition was initiated. The first generation of FLT3 inhibitors (e.g. midostaurin, sorafenib, sunitinib) displayed a broad spectrum of kinase inhibition. This was extended over time by a second generation of more selective FLT3 inhibitors (e.g. quizartinib, gilteritinib, FF-10101). Several candidates from both generations successfully underwent clinical trials and being approved for AML treatment (midostaurin [4] and gilteritinib [5] received FDA approval, and quizartinib [6] was approved by regulatory authority in Japan). Nevertheless, the duration of FLT3 inhibitor-induced response is frequently limited due to the resistance development and subsequent relapse [7].

Strategies trying to deal with the resistance onset after FLT3 inhibitor therapy including combinations with conventional chemotherapy or haematopoietic stem cell transplantations are currently tested [8],

* Corresponding author. Department of Experimental Biology, Faculty of Science, Palacký University Olomouc, Šlechtitelů 27, 78371, Olomouc, Czech Republic.
** Corresponding author.
E-mail addresses: miroslav.soural@upol.cz (M. Soural), vladimir.krystof@upol.cz (V. Kryštof).
[1] Both authors contributed equally.

https://doi.org/10.1016/j.ejmech.2022.114792
Received 8 August 2022; Received in revised form 13 September 2022; Accepted 21 September 2022
Available online 26 September 2022

however novel approaches are still needed. Specific degradation of FLT3 via proteolysis targeting chimeras (PROTACs) could provide an alternative approach to overcome the limitations in AML treatment associated with the fast mutational rate of FLT3 gene. First described in 2001 [9], PROTACs are heterobifunctional conjugates consisting of a protein of interest (POI) binder interconnected to a ligand capable of E3 ubiquitin ligase engagement. PROTACs form a ternary complex with both these proteins resulting in polyubiquitination of the POI and inducing its degradation via proteasome. PROTACs provide some advantages over conventional kinase inhibitors. For example, owing to PROTAC's ability to work as a catalyser to degrade a target protein and given that E3 ligases have high enzymatic turnover, the cells usually require only low PROTAC exposure to give high cellular and in vivo efficacy. In addition, the effects can have long duration, so the drug exposure could be lower. And finally, some target enzymes display non-enzymatic scaffolding functions, which cannot be addressed by simple inhibition [10].

FLT3-recruiting PROTACs have been developed by groups of Gray [11] and Crews [12] in 2018 whose conjugates were based on FLT3-selective inhibitor quizartinib linked to cereblon (CRBN) and von Hippel-Lindau (VHL) ligands, respectively (Fig. 1A and B). Two other PROTACs based on tyrosine kinase inhibitor dovitinib [13] or experimental pyrrolo[2,3-*d*]pyrimidine derivative [14] were developed later on. These studies demonstrate that FLT3-ITD is amenable to degradation and that FLT3-targeting PROTACs provide efficacious compounds, further confirming the potential of this approach.

Although FLT3 as the most common driver of AML is undoubtedly suitable therapeutic option, the urgent need for more effective therapy expands the range of discussed targets for drug intervention including CDK9 [15]. Serine-threonine protein kinase CDK9 is a key regulator of transcriptional initiation and elongation having a great impact on levels of key prosurvival and apoptotic factors. Several studies highlight positive effect of CDK9 inhibition alone [16,17] or with simultaneous inhibition of other target including FLT3 [18]. Combination with other compounds such as Bcl-2 inhibitor venetoclax [19,20] in different haematological malignancies counting AML have been reported as well.

Encouraged by these facts, we decided to incorporate a potent kinase inhibitor from the recently described 2,6,9-trisubstituted purine series [21] into PROTAC conjugate. The lead compound of the 2,6,9-trisubstituted purine series showed significant selectivity to AML cell lines bearing the FLT3-ITD mutation. It blocked the autophosphorylation of FLT3 and inhibited its downstream signalling leading to G1 cell cycle phase arrest and apoptosis [21]. In addition to outstanding FLT3 inhibitory properties, it also displayed activity towards CDK9. In this manuscript, we describe a PROTAC based on purine inhibitor **BPA311**, targeting both FLT3 and CDK9, two independent relevant AML cellular targets, with strong activity and selectivity towards FLT3-ITD expressing AML cell lines.

2. Results and discussion

2.1. Molecular design

Molecular docking studies, as well as inspections of available co-crystals with analogous kinase inhibitors [22–24], have indicated the orientation of **BPA311** (Fig. 1C) in the ATP active site of FLT3 and CDK9 kinases (Fig. 1D). Importantly, 4-ethyl-piperazin-1-yl-phenyl moiety of the compound pointed outward from the active site, thus the *N*-ethyl-piperazine part provided a rational option for enlarging the ethyl chain to a linker bound to pomalidomide, a CRBN ligand successfully applied in several protein kinase targeting PROTACs. Next, a suitable way of conjugation was established, as is known that the linker composition and its attachment to the ligand play a critical role in the successful development of PROTAC degraders [25,26]. The current synthetic toolbox offers a number of strategies for PROTAC construction; however, for practical reasons, we initially applied the readily available thalidomide-preloaded resin (TPR) [27], which enables fast and simple conjugation with the reactive amine-containing inhibitors. For this purpose, compound **7**, with the free piperazine moiety, was synthesized (Scheme 1) and subjected to conjugation using TPR which provided the corresponding PROTAC **S19** (see Scheme S1 and Fig. S1 in Supplementary material for details). Nevertheless, a negative outcome was detected in the degradation assay (Fig. S1B) pointing to a non-optimal structure of the PROTAC conjugate. Subsequently, instead of the typical "trial-and-error" approach, consisting of the preparation of a series of PROTACs with different linker lengths, we attempted to rationally design the optimal structure using molecular modelling and clues from the previously reported degraders [11,12,28]. The outcome of this procedure clearly indicated the need for a shorter linker, and eventually changing the type of attachment. Consequently, PROTAC **13** (Fig. 1E and Scheme 2) was designed with the spacer resembling the structure of quizartinib-CRBN PROTAC (Fig. 1A) [11].

2.2. Preparation of PROTAC components: modified BPA311 and pomalidomide-glycine (Pom-Gly)

The synthetic strategy started with derivatization of 1-(4-

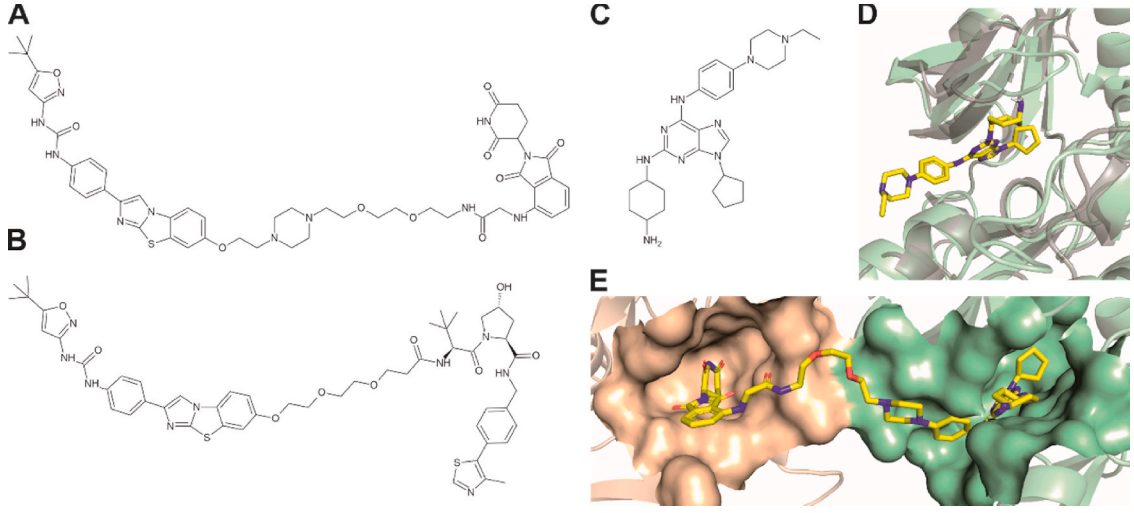

Fig. 1. Published FLT3 PROTAC conjugates: Quizartinib linked to CRBN (A) and VHL (B) ligands. Design of PROTAC: (C) Structure of FLT3-ITD/CDK9 inhibitor **BPA311**. (D) Overlay of FLT3 (green) and CDK9 (grey) with **BPA311** in the active site. (E) Predicted binding of PROTAC **13** (yellow) to FLT3 (green) and CRBN (orange).

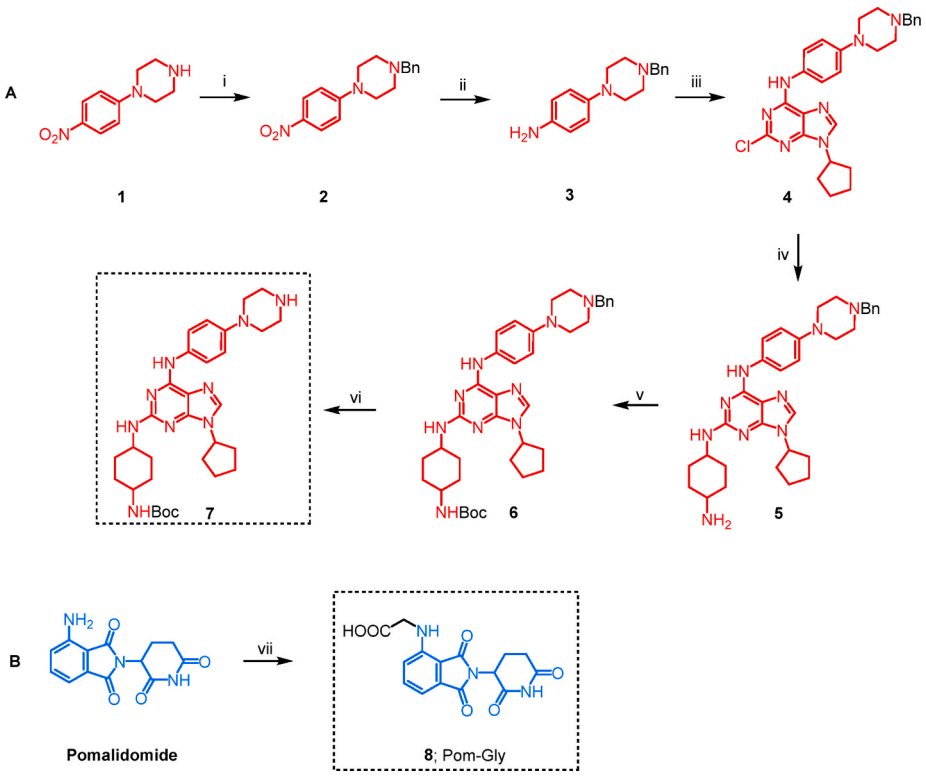

Scheme 1. Synthesis of purine ligand **7** and pre-modified pomalidomide **8**. *Reagents and conditions:* (i) benzyl bromide, K_2CO_3, DMF/CH_3CN, 50 °C, 3 h; (ii) PtO_2, ethanol/THF, r.t., 90 min; (iii) 2,6-dichloro-9-cyclopentyl purine, *N,N*-diisopropylethylamine (DIPEA), DMSO, 120 °C, 16 h; (iv) *trans*-1,4-diaminocyclohexane, DIPEA, diethylene glycol diethyl ether, 160 °C, 24 h; (v) Boc_2O, Et_3N, 4-(dimethylamino)pyridine (DMAP), THF, r.t., 16 h; (vi) NH_4HCO_2, Pd/C, ethanol, 80 °C, 16 h; (vii) glyoxylic acid, Bu_2SnCl_2, phenyl silane, THF, reflux, 16 h.

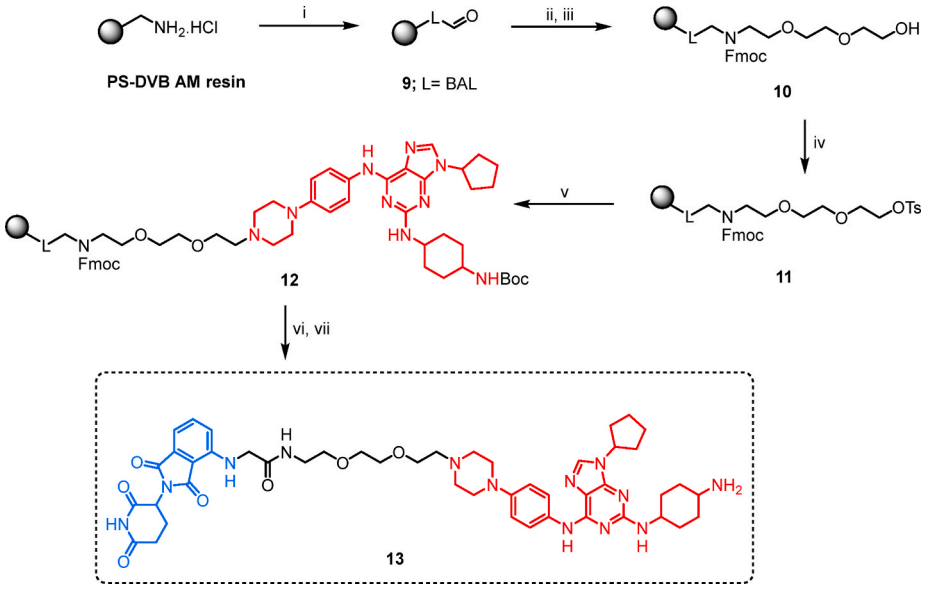

Scheme 2. Synthesis of PROTAC **13**. *Reagents and conditions:* (i) 4-(4-formyl-3-methoxyphenoxy)butanoic acid, 1-hydroxybenzotriazole (HOBt), *N,N′*-diisopropylcarbodiimid (DIC), DMF/CH_2Cl_2, r.t., 16 h; (ii) 2-(2-(2-aminoethoxy)ethoxy)ethan-1-ol, DMF/AcOH, r.t., 16 h then $NaBH(OAc)_3$, DMF/AcOH, r.t., 4 h; (iii) Fmoc-OSu, CH_2Cl_2, r.t., 16 h; (iv) tosyl chloride (TsCl), Et_3N, DMAP, CH_2Cl_2, r.t., 16 h; (v) **7**, DIPEA, DMF, 70 °C, 16 h; (vi) a) 1,8-diazabicyclo [5.4.0]undec-7-ene (DBU)/CH_2Cl_2, r.t., 10 min, b) **8**, HOBt, DIC, DMF, r.t., 16 h; (vii) TFA/CH_2Cl_2, r.t., 2 h.

nitrophenyl)piperazine **1**. This compound was in two steps converted to 4-(*N*-benzyl)piperazine aniline **3**, which underwent regioselective aromatic nucleophilic substitution with 2,6-dichloro-9-cyclopentyl-purine to yield intermediate **4** (Scheme 1A). The choice of benzyl protecting group was carefully envisioned for orthogonal manipulation in the presence of acid-labile *t*-butoxycarbonyl (Boc) group later in the sequence.

Installation of cyclohexyl diamine motif to the C^2 purine position was inspired by our previous work [29]. However, the Buchwald-Hartwig cross-coupling was not successful in this case and only starting material **4** was recovered under various conditions. In contrast, using large excess of diamine at harsh conditions (160 °C) yielded the desired intermediate **5** (Scheme 1A). The diamine moiety was then protected with the Boc protecting group, removable under acidic conditions during the cleavage of the final PROTAC from the resin (see later in the text, Scheme 2). Finally, deprotection of the benzyl group under ammonium formate-promoted *in situ* hydrogenation in a presence of palladium on activated charcoal (Pd/C) yielded final purine ligand **7** (Scheme 1A). The modification of pomalidomide was achieved by silane-based direct reductive amination [30] with glyoxylic acid that yielded Pom-Gly **8** (Scheme 1B).

2.3. Preparation of the PROTAC

To prepare the desired conjugate, the solid-phase synthesis was used as it allowed simple and fast preparation of the targeted compound in a multistep sequence without the need of tedious purification. The synthesis started from commercially available amino methyl polystyrene (PS-DVB AM) resin which was in the first step equipped with backbone amide linker (BAL) using 4-(4-formyl-3-methoxyphenoxy)butanoic acid (Scheme 2). Subsequent reductive amination in the presence of 2-(2-(2-aminoethoxy)ethoxy)ethan-1-ol and $NaBH(OAc)_3$ was followed by protection with fluorenylmethyloxycarbonyl (Fmoc) protecting group which yielded intermediate **10**. After tosylation, the nucleophilic substitution with prepared purine ligand **7** yielded intermediate **12**. The reaction proceeded smoothly; however, high temperature was needed to reach full conversion to the product. Notably, we also observed partial cleavage of Fmoc during this step, due to the excess of DIPEA used. A quantitative deprotection was accomplished with the mixture of DBU/CH_2Cl_2, which proved itself as the superior alternative to standard piperidine/DMF cocktail [27]. Acylation with Pom-Gly **8** was followed by cleavage from the resin with concomitant removal of Boc protecting group which yielded desired PROTAC **13** (Scheme 2).

2.4. Antiproliferative activity and protein kinase selectivity

PROTAC **13** displayed significant antiproliferative selectivity against AML cell lines bearing FLT3-ITD mutation (MV4-11 and MOLM-13) with the GI_{50} values ranging in nanomolar concentrations while the GI_{50} values obtained for the FLT3-independent leukaemic cells were at least 20 times higher. Although potency of PROTAC **13** did not improve over parent **BPA311**, it maintained the selectivity towards the FLT3-ITD expressing leukaemic cells (Table 1). Importantly, a twofold difference in the GI_{50} values measured in MV4-11 and CRBN-deficient MV4-11 [31] suggested the activity at least partly associated with CRBN-dependent mechanism of action.

The selectivity of PROTAC **13** was compared to its parent compound **BPA311** in the panel of 46 kinases across the human kinome at 100 nM concentration. The results indicated that PROTAC **13** maintained the activity of parent molecule towards FLT3 (2% residual activity in both compounds) as well as CDK9 (3% and 8% residual activity, respectively) (Fig. S2).

2.5. Cellular effects

Conventional FLT3-kinase inhibitors act through inhibition of the FLT3 autophosphorylation and subsequent dampening of its downstream signalling pathways, namely MAPK-ERK and STAT5 pathways. This results in block of proliferation of FLT3-dependent cells while such compounds do not affect other cells. However, additional effects of these compounds can be seen in the levels of FLT3 protein itself. Cells bearing FLT3-ITD mutation are characterized by predominant intracelullar localization of the immature 130-kDa form of FLT3, which is not fully glycosylated [32,33]. Long-term treatment with FLT3 inhibitors induces glycosylation, maturation, and subsequent FLT3 translocation to the cell surface and its anchoring to the cytoplasmic membrane. Moreover, these changes are linked with increased FLT3 protein levels caused by elevated FLT3 mRNA expression [33] having a potential impact on a resistance development in the long-term perspective [34]. This outcome was proved in our experiment performed on MV4-11 cells bearing the FLT3-ITD mutation (Fig. 2A). Overnight treatment with FLT3 inhibitors quizartinib and sorafenib reduced the autophosphorylation of FLT3 at Y589/591 and suppressed signalling of its downstream pathways that was proved by decreased phosphorylation of ERK1/2 at T202/Y204 as well as STAT5 at Y694. A similar effect was observed after treatment with PROTAC **13** that proved the binding of the conjugate into the FLT3 active site. Quizartinib as well as sorafenib significantly increased the total level of FLT3, on the other hand, levels of FLT3 after treatment with low nanomolar concentrations of PROTAC **13** remained comparable with endogenous levels in untreated cells; concentrations of 100 nM and higher induced FLT3 degradation. The degradation of protein levels in a concentration-dependent manner was observed also in the case of CDK9, which were not affected by quizartinib nor sorafenib. Comparable results were obtained in heterozygous FLT3-ITD cell line MOLM-13 (Fig. S3).

To confirm a CRBN-dependent mechanism of action, the previous experiment was repeated using CRBN-deficient MV4-11 (Fig. 2B and S4) [31]. Identical results were obtained with control samples of quizartinib- and sorafenib-treated cells. Both inhibitors blocked the FLT3-dependent signalling efficiently and induced upregulation of FLT3 protein. Absence of CRBN resulted in the prevention of E3 ligase engagement of PROTAC **13**. Target proteins were not ubiquitinated and their levels were not decreased by proteasome-mediated degradation. While the CDK9 levels remained unaltered, the concentration-dependent stabilization of FLT3 that is typical for FLT3 kinase inhibitors was observed.

In addition, proapoptotic effects of PROTAC **13** depending on CRBN levels in MV4-11 cells were evaluated. Activities of caspases 3 and 7, key executioner players of apoptotic cascade, were measured in MV4-11 as well as CRBN-deficient MV4-11 cells treated with PROTAC **13**, quizartinib and sorafenib for 16 h using the fluorescently labelled peptide substrate Ac-DEVD-AMC (Fig. 3). In MV4-11 cells, we observed massive concentration-dependent activation of caspases upon PROTAC **13** treatment that was in line with cleavage of protein PARP-1, a substrate of caspases (Fig. 2). Contrary to this, 100 nM concentrations of quizartinib and sorafenib showed only minimal effect on activation of caspases in MV4-11 cells. In CRBN-deficient MV4-11 cells, PROTAC **13**-induced activation of caspases was not observed and measured activities were at the endogenous level of the untreated control sample. These results were repeated by an alternative approach and complemented with MOLM-13 (FLT3-ITD) and THP-1 (FLT3 wild-type) cell lines confirming the sensitivity of FLT3-ITD bearing cells to targeted degradation of FLT3 and CDK9 (Fig. S5).

These results were also confirmed using flow cytometry analysis (Fig. S6). Although the effect of PROTAC **13** on cell cycle phase distribution was comparable between MV4-11 and CRBN-deficient MV4-11 cells, and we observed concentration-dependent increase of the cells arrested in the G1 phase of the cell cycle that is typical for FLT3 inhibition, the MV4-11 cells were far more sensitive to the treatment. Higher tested concentrations induced apoptosis in the MV4-11 cells resulting in the massive increase of the subG1 population, while the CRBN-deficient counterpart cells were not affected and the proapoptotic effect of PROTAC **13** was not confirmed in this model. These results suggest that the cells are more sensitive to degradation of the target proteins rather than only to kinase inhibition.

The effect of PROTAC **13** on CDK9, a key transcriptional regulator, has a potential to be transmitted into the reduced expression of genes

Table 1
Antiproliferative activity of PROTAC **13** and compound **BPA311** in panel of leukaemic cell lines.

cell line	GI_{50} ± SD (μM)[a]	
	PROTAC 13	BPA311
MV4-11	0.047 ± 0.029	0.009 ± 0.007
MV4-11 CRBN-def.	0.119 ± 0.039	0.008 ± 0.004
MOLM-13	0.042 ± 0.031	0.008 ± 0.011
RS4-11	1.014 ± 0.208	0.295 ± 0.062
HL60	6.122 ± 2.383	1.520 ± 0.074
U937	9.507 ± 0.641	0.695 ± 0.224
THP-1	9.993 ± 0.012	0.681 ± 0.139
Kasumi-1	>10	0.534 ± 0.001
CEM	>10	1.278 ± 0.073
K562	>10	2.070 ± 0.490

[a] GI_{50} determined after 72 h cultivation.

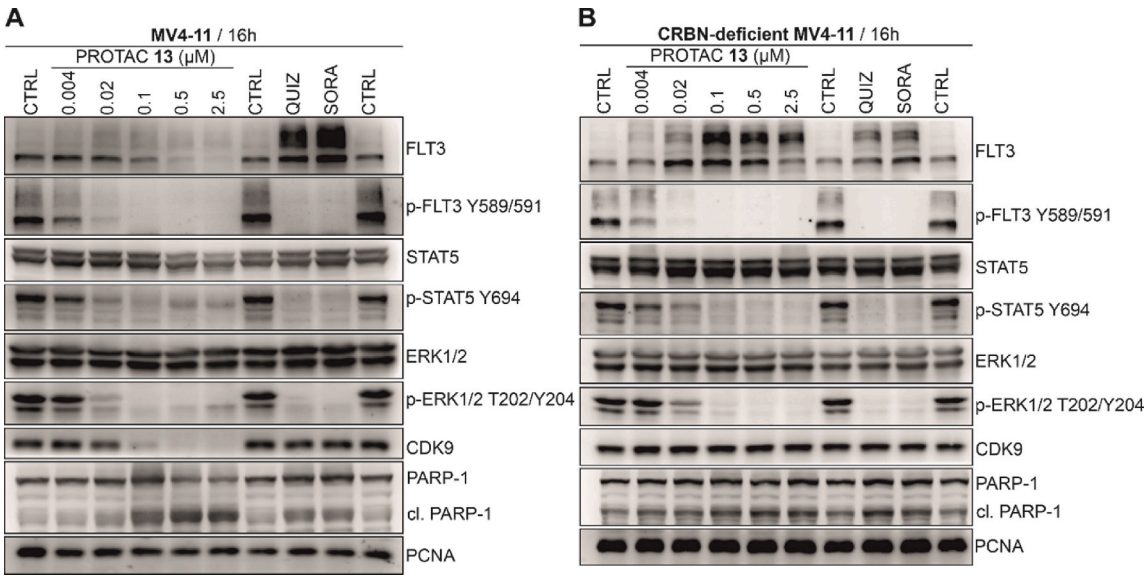

Fig. 2. Immunoblotting analysis of MV4-11 (A) and CRBN-deficient MV4-11 (B) cells treated with PROTAC **13**. Quizartinib (QUIZ) and sorafenib (SORA) at 0.1 μM concentration were used as controls.

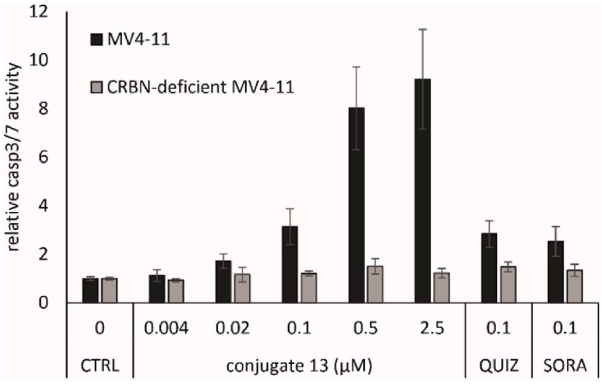

Fig. 3. Induction of apoptosis in MV4-11 and CRBN-deficient MV4-11 cells treated with PROTAC **13**, quizartinib (QUIZ) and sorafenib (SORA).

involved in AML pathogenesis. To confirm this we selected genes essential for haematopoiesis, apoptosis and AML initiation including HOXA9, MEIS1, MCL-1, Bcl-2, Myc and Myb whose expression, moreover, often correlates with poor prognosis of the disease. MV4-11 cells were treated for 4 h with increasing concentrations of PROTAC **13**, which showed dose-dependent ability to affect significantly the expression of all studied genes (Fig. 4). On the other hand, quizartinib and sorafenib did not show such a strong impact. These results indicate another potential therapeutic benefit of CDK9 targeting in AML. In addition, levels of FLT3 transcripts were not affected by PROTAC **13** treatment further confirming its mechanism of action.

To further verify the PROTAC-mediated mechanism of action, MV4-11 cells were pre-treated with 4-hydroxythalidomide as the CRBN ligand to limit the ternary complex formation. 4-Hydroxythalidomide itself had no impact on MV4-11 cells, levels of target proteins remained unaltered and FLT3 signalling pathway was not affected as well. PROTAC **13** induced massive degradation of FLT3 and CDK9. While the 4-hydroxythalidomide pre-treatment did not affect the binding of PROTAC **13** into the kinase active sites, as proved by inhibition of FLT3 autophosphorylation as well as reduction of downstream signalling pathways, the CRBN binding site was blocked and thus the ternary complex formation was abolished. The CDK9 degradation caused by PROTAC **13** was significantly reduced by 4-hydroxythalidomide pre-treatment, and FLT3 levels were even elevated, as is typical for standard FLT3 kinase inhibitors (Fig. 5A).

Interestingly, the proapoptotic effect of PROTAC **13** that was confirmed using caspase-3/7 fluorimetric-based assay in MV4-11 treated lysates was shown to be repressed by 4-hydroxythalidomide pre-treatment and activity of caspase-3/7 in these samples remained significantly lower (Fig. 5B). These results further proved beneficial properties of PROTAC **13**.

Alternatively, PROTAC-induced effects should be abolished by proteasome inhibition. Nevertheless, proteasome inhibitors are known to induce degradation of FLT3-ITD in AML cells [35], complicating the experimental setup. We therefore decided to find a suitable compound tool which, in the proper concentration, would block proteasome activity without adverse effects on FLT3-ITD and CDK9 levels. Among the tested inhibitors (data not shown), results of MG132 at concentration of 200 nM were the most convenient. In MV4-11 cells treated with MG132 alone, we observed significantly increased levels of polyubiquitinated proteins indicating proteasome function failure, while the CDK9 and FLT3 protein levels were not decreased dramatically in comparison to untreated control cells. The observed degradation of target proteins caused by PROTAC **13** was diminished when the MV4-11 cells were pre-treated for 90 min with MG132 prior to PROTAC **13** treatment (Fig. 6). These results confirm the proteasome-dependent degradation of the target proteins caused by our conjugate.

3. Conclusion

AML belongs to the most devastating haematological malignancies whose onset was shown to be often linked to oncogenic mutations in the gene encoding FLT3. Internal tandem duplications and mutations in the kinase domain in FLT3 can be detected in a third of all patients with AML diagnosis. Although several kinase inhibitors showing potency and selectivity towards FLT3-ITD expressing AML were developed, their efficacy is often reduced by resistance development and relapse of the disease. This can be avoided by use of resistance-overcoming inhibitors of new generations or by co-targeting of FLT3 and other relevant target, which plays a role in cancer cells survival. Emerging PROTAC-mediated protein degradation offers another potential therapeutic strategy enabling elimination of oncogenic targets by a mechanism different from available competitive kinase inhibition.

By combining our previously reported FLT3/CDK9 kinase inhibitor

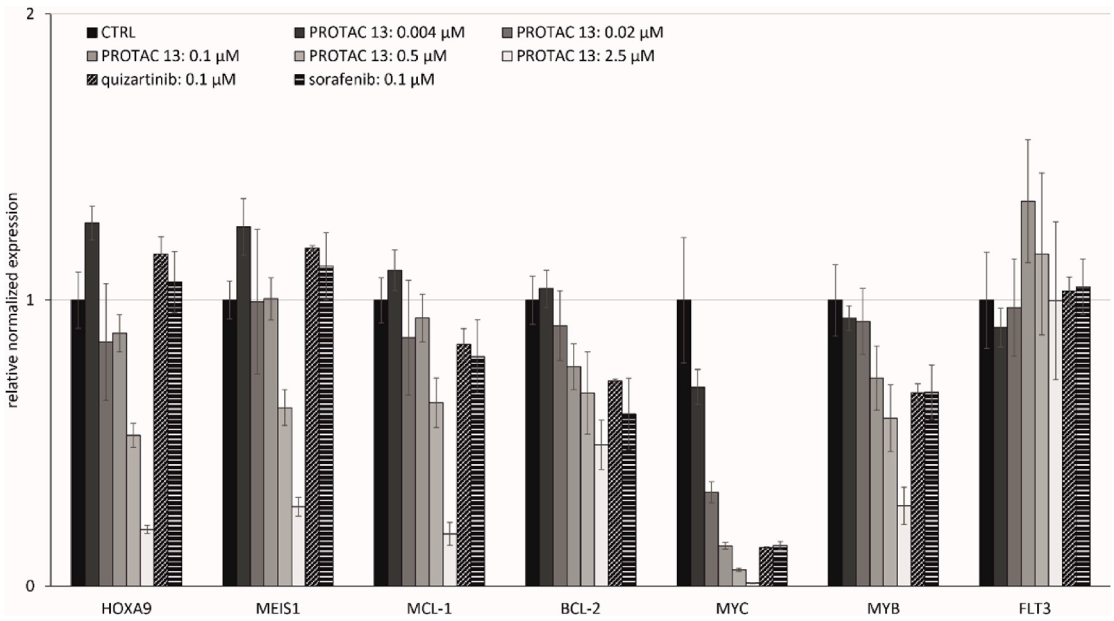

Fig. 4. Relative normalized expression of HOXA9, MEIS1, MCL-1, BCL-2, MYC, MYB and FLT3 genes in MV4-11 cells. MV4-11 cells were treated with PROTAC **13**, quizartinib or sorafenib for 4 h. Gene expressions were normalized per GAPDH and RPL13A genes.

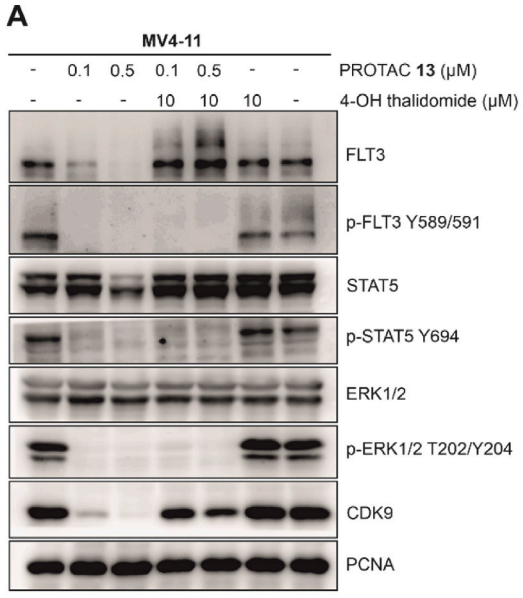

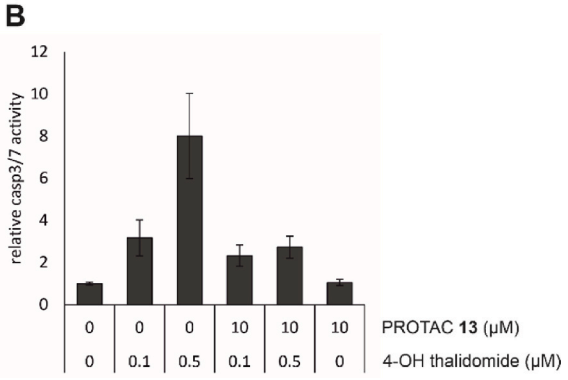

Fig. 5. Effects of PROTAC **13** on levels of FLT3 and CDK9 (A) as well as its proapoptotic activities (B) in MV4-11 cells are reversed by competition with 4-hydroxythalidomide. Cells were pre-treated with 10 μM 4-hydroxythalidomide for 90 min and treated with PROTAC **13** for further 16 h.

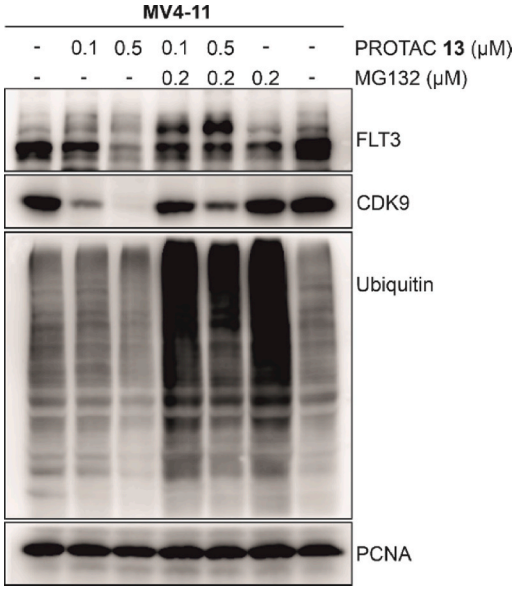

Fig. 6. Inhibition of proteasome blocks the degradation of FLT3 and CDK9 caused by PROTAC **13** in MV4-11 cells. Cells were pre-treated with 0.2 μM MG132 for 90 min and treated with PROTAC **13** for further 16 h.

with CRBN-ligand pomalidomide, we have obtained PROTAC **13** showing significant selectivity towards FLT3-ITD-mutated AML cells. Although potency of PROTAC **13** did not improve over parent inhibitor, it acted by a new CRBN-dependent mechanism of action. PROTAC **13** efficiently blocked FLT3 and its downstream signalling pathways that are important for proliferation as well as survival of FLT3-dependent leukaemic cells. In addition, transcriptional repression caused by CDK9 degradation reduced expression of genes playing crucial roles in AML pathogenesis and correlating with poor disease prognosis. Results indicate that FLT3-ITD expressing cells are more sensitive to FLT3 and CDK9 degradation caused by PROTAC **13**-mediated mechanism of action than only to their kinase inhibition. This induces activation of an apoptotic cascade and cell death. We believe that the simultaneous

degradation of FLT3 and CDK9 could be the beneficial option for AML therapy.

4. Experimental section

4.1. General information

All reagents were of reagent grade and used without further purification. Solvents and chemicals were purchased from Sigma-Aldrich (US), Acros Organics (Belgium) or Fluorochem (UK). Anhydrous solvents were dried over 4 Å molecular sieves or stored as received from commercial suppliers.

Reactions on solid-phase were performed in plastic syringes, each equipped with a porous disk, using a manually operated synthesizer (Torviq, US), unless otherwise stated. The volume of wash solvent was 10 mL per 1 g of resin. For washing, resin slurry was shaken with the fresh solvent for at least 1 min before changing the solvent. Resin-bound intermediates were dried under a stream of nitrogen for prolonged storage and/or quantitative analysis. For the UHPLC-MS analysis a sample of resin (~5 mg) was treated with CH_2Cl_2/TFA (1:1, 1 mL, v/v), the cleavage cocktail was evaporated under a stream of nitrogen, and cleaved compounds extracted into CH_3CN/H_2O (1:1, 1 mL, v/v).

Reactions in solution-phase were performed in round-bottom flasks fitted with rubber septa under positive pressure of nitrogen or in ace-pressure tubes, unless otherwise stated. All reactions were monitored by UHPLC-MS analysis. Thin-layer chromatography (TLC) plates using aluminium plates precoated with silica gel (silica gel 60 F_{254}, Merck, US) impregnated with a fluorescent indicator were visualized by exposure to ultraviolet light ($\lambda = 254$ nm) and/or by submersion in aqueous ceric ammonium molybdate (CAM) solution followed by brief heating. Column chromatography was performed using silica gel (60 Å, 230–400 mesh, Sigma-Aldrich).

Prior to HPLC separation (column Phenomenex Gemini, 50 × 2.00 mm, 3 μm particles, C^{18}), the samples were injected by direct infusion into the mass spectrometer using autosampler. Mobile phase was isocratic 80% CH_3CN and 20% 0.01 M ammonium acetate in H_2O or 95% methanol +5% H_2O + 0.1% formic acid and flow 0.3 mL/min.

4.2. Instrumentation

UHPLC-MS analyses were carried out on UHPLC-MS system consisting of UHPLC chromatograph Acquity with photodiode array detector and single quadrupole mass spectrometer (Waters, US), using X-Select C^{18} column at 30 °C and flow rate of 0.6 mL/min. Mobile phase was (A) 0.01 M ammonium acetate in H_2O, and (B) CH_3CN, linearly programmed from 10% A to 80% B over 2.5 min, kept for 1.5 min. The column was re-equilibrated with 10% of solution B for 1 min. The ESI source operated at discharge current of 5 μA, vaporizer temperature of 350 °C and capillary temperature of 200 °C. HPLC purification was carried out on C^{18} reverse phase column (YMC Pack ODS-A, 20 × 100 mm, 5 μm particles), gradient was formed from CH_3CN and 0.01 M ammonium acetate in H_2O, flow rate 15 mL/min. For lyophilization of residual solvents at −110 °C the ScanVac Coolsafe 110-4 was used.

HRMS analyses were performed using LC chromatograph (Dionex Ultimate 3000, Thermo Fischer Scientific, US) and Exactive Plus Orbitrap high-resolution mass spectrometer (Thermo Fischer Scientific, US) operating at positive full scan mode (120 000 FWMH) in the range of 100–2000 *m/z*. The settings for electrospray ionization were as follows: oven temperature of 150 °C and source voltage of 3.6 kV. The acquired data were internally calibrated with phthalate as a contaminant in methanol (*m/z* 297.15909). Samples were diluted to a final concentration of 0.1 mg/mL in CH_3CN/H_2O (9:1, v/v).

NMR spectra were recorded on JEOL ECX500 spectrometer at magnetic field strengths of 11.75 T with operating frequencies 500.16 MHz (for ^1H) and 125.77 MHz (for ^{13}C) at 27 °C. Chemical shifts (δ) are reported in parts per million (ppm) and coupling constants (*J*) are reported in Hertz (Hz). The ^1H and ^{13}C NMR chemical shifts (δ in ppm) were referenced to the residual signals of DMSO-d_6 [2.50 (^1H) and 39.52 (^{13}C)]. The residual signal of ammonium acetate (from HPLC purification) exhibited signal at 1.90 ppm (^1H) and at 21.3 ppm and 172.0 ppm (^{13}C). Abbreviations in NMR spectra: app – apparent, br s – broad singlet, d – doublet, dd – doublet of doublets, m – multiplet, p – pentet, s – singlet, t – triplet.

4.3. Experimental procedures

4.3.1. Procedure for benzylation

To a stirred solution of 1-(4-nitrophenyl)piperazine **1** (1 g, 4.83 mmol, 1 eq) in anhydrous DMF/CH_3CN (3:1, 15 mL, v/v) were added benzyl bromide (860 μL, 7.24 mmol, 1.5 eq) and K_2CO_3 (1.3 g, 9.66 mmol, 2 eq). The reaction mixture was stirred at 50 °C for 3 h after which UHPLC-MS confirmed full conversion to compound **2**. The reaction mixture was concentrated, diluted with aq. NH_4Cl (250 mL), and extracted with EtOAc (3 × 250 mL). Organic extracts were combined, dried over $MgSO_4$, filtered, and evaporated under reduced pressure. The crude product was purified by column chromatography (CH_2Cl_2/EtOAc 1:1, v/v) to afford compound **2** as yellow solid (931 mg, 65% yield).

4.3.2. Procedure for reduction of nitro group

The starting material 2 (359 mg, 1.21 mmol, 1 eq) was dissolved in a mixture of anhydrous ethanol/THF (3:1, 8 mL v/v) and properly flushed with nitrogen for 15 min. Then, PtO_2 (192 mg, 0.85 mmol, 0.7 eq) was added, and the resulting mixture was stirred at ambient temperature under positive pressure of hydrogen. UHPLC-MS analysis was used to confirm the full conversion to the corresponding product after 90 min. The reaction mixture was diluted with methanol, and residual PtO_2 was filtered off. The residual solvents were evaporated under reduced pressure, and crude product **3** (510 mg, 1.91 mmol) was used to the next step without further purification.

4.3.3. Procedure for alkylation of 2,6-dichloropurine

2,6-dichloro-9-cyclopentyl purine was prepared by previously published procedure [29].

4.3.4. Procedure for aromatic nucleophilic substitution with *3*

To a stirred solution of **3** (510 mg, 1.91 mmol, 1.1 eq) in anhydrous DMSO (8 mL) were added 2,6-dichloro-9-cyclopentyl purine (446 mg, 1.73 mmol, 1 eq) and DIPEA (315 μL, 1.91 mmol, 1.1 eq). The reaction mixture was stirred at 120 °C for 16 h after which UHPLC-MS confirmed full conversion to product **4**. The reaction mixture was cooled down to ambient temperature, diluted with aq. NH_4Cl (200 mL), and extracted with EtOAc (3 × 200 mL). Organic extracts were combined, dried over $MgSO_4$, filtered and evaporated under reduced pressure. The crude product was purified by column chromatography (CH_2Cl_2/MeOH gradually eluted from 15:1 to 5:1, v/v) to afford compound **4** as pale brown solid (501 mg, 60% yield).

4.3.5. Procedure for aromatic nucleophilic substitution with diamine

Starting material **4** (254 mg, 0.52 mmol, 1 eq) in ace-pressure tube was dissolved in diethylene glycol diethyl ether (4 mL). Then, solid *trans*-1,4-diamino cyclohexane (2.9 g, 26 mmol, 50 eq) was added at once to the solution of starting material, followed by addition of DIPEA (2.5 mL). The reaction mixture was vigorously stirred at 160 °C for 22 h after which UHPLC-MS confirmed full conversion to product **5**. The reaction mixture was cooled down to ambient temperature, diluted with CH_3CN (20 mL) upon which residual solid precipitated and was filtered off. The residual solvents were concentrated under reduced pressure and lyophilized overnight. The crude product was purified by column chromatography (CH_2Cl_2/7 M NH_3 in MeOH 10:1, v/v) to afford compound **5** as pale brown solid (200 mg, 67% yield).

4.3.6. Procedure for protection with Boc

To a stirred solution of starting material **5** (126 mg, 0.22 mmol, 1 eq) and Et_3N (50 μL, 0.35 mmol, 1.6 eq) in anhydrous THF (2 mL) at 0 °C was added DMAP (4 mg, 0.03 mmol, 15 mol%) in anhydrous THF (500 μL). The reaction mixture was stirred for 3 min when solution of Boc_2O (60 mg, 0.27 mmol, 1.2 eq) in anhydrous THF (500 μL) was added and the mixture was warmed up to ambient temperature. The reaction mixture was stirred for 16 h after which UHPLC-MS confirmed full conversion to product **6**. The residual solvents were evaporated under reduced pressure and crude product was purified by column chromatography (CH_2Cl_2/MeOH 10:1, v/v) to obtain compound **6** as colourless oil (135 mg, 92% yield).

4.3.7. Procedure for cleavage of benzyl group

To a stirred solution of NH_4HCO_2 (504 mg, 8 mmol) in anhydrous ethanol (15 mL) was added solution of starting material **6** (146 mg, 0.22 mmol, 1 eq) in anhydrous ethanol (5 mL) and palladium on activated charcoal (10% of Pd, 26 mg, 0.24 mmol, 1.1 eq). The resulting mixture was stirred at 80 °C for 36–42 h after which UHPLC-MS confirmed full conversion to product **7**. The reaction mixture was cooled down to ambient temperature, diluted with ethanol and residual catalyst was filtered off. The solvents were evaporated, and the crude product was purified by column chromatography (CH_2Cl_2/MeOH gradually eluted from 15:1 to 5:1, v/v) to obtain compound **7** as a pale yellow solid (86 mg, 68% yield).

4.3.8. Procedure for reductive amination in solution phase

Pomalidomide (250 mg, 0.92 mmol, 1 eq) was dissolved in THF (15 mL), followed by addition of glyoxylic acid monohydrate (421 mg, 4.57 mmol, 5 eq) and Bu_2SnCl_2 (278 mg, 0.92 mmol, 1 eq). The mixture was vigorously stirred for 20 min at ambient temperature and then phenyl silane (562 μL, 4.57 mmol, 5 eq) was slowly added. The reaction mixture was heated up to reflux and stirred for 22 h after which UHPLC-MS analysis confirmed full conversion to product **8**. The mixture was cooled down to ambient temperature, diluted with aq. NH4Cl (200 mL) and extracted with EtOAc (3 × 200 mL). Organic extracts were combined, dried over MgSO4, filtered and evaporated under reduced pressure. The crude product was purified by column chromatography (CH_2Cl_2/MeOH/AcOH 10:1:0.2, v/v) to afford compound **8** as yellow solid (260 mg, 86% yield).

4.3.9. Procedure for preparation of BAL resin

Amino methyl polystyrene resin (1 g, loading 0.98 mmol/g) was swollen in CH_2Cl_2 (10 mL) for 30 min, washed with DMF (3 × 10 mL), neutralized in DMF/piperidine (5:1, 10 mL) for additional 30 min and then again washed with DMF (5 × 10 mL). 4-(4-formyl-3-methoxyphenoxy)butanoic acid (700 mg, 2.94 mmol) and HOBt (450 mg, 2.94 mmol) were dissolved in DMF/CH_2Cl_2 (1:1, 10 mL, v/v) and DIC (460 μL, 2.94 mmol) was added. The resulting solution was added to the polypropylene fritted syringe with amino methyl polystyrene resin. The reaction slurry was shaken at ambient temperature for 16 h, followed by wash with DMF (3 × 10 mL) and CH_2Cl_2 (3 × 10 mL). Negative bromophenol blue test confirmed quantitative acylation of the resin.

4.3.10. Procedure for reductive amination and Fmoc-protection on solid-phase

BAL resin **9** (500 mg, loading 0.98 mmol/g) was swollen in CH_2Cl_2 (5 mL) for 30 min, then washed with anhydrous THF (3 × 5 mL) and anhydrous DMF (3 × 5 mL). The solution of 2-(2-(2-aminoethoxy) ethoxy)ethan-1-ol (338 μL, 2.45 mmol) in DMF/AcOH (10:1, 5 mL, v/v) was added to polypropylene fritted syringe with BAL resin **9** and it was shaken for 16 h at ambient temperature. Then, $NaBH(OAc)_3$ (309 mg, 1.47 mmol) in DMF/AcOH (20:1, 5 mL, v/v) was added portion wise (3 × 103 mg) to the reaction mixture during the period of 4 h. The reaction slurry was shaken at ambient temperature for 16 h, followed by washing with DMF (5 × 5 mL), CH_2Cl_2 (3 × 5 mL), neutralization with DMF/Et_3N (10:1, 5 mL, v/v) for additional 30 min and final wash with CH_2Cl_2 (3 × 5 mL). Fmoc-OSu (1 g, 3 mmol) was dissolved in CH_2Cl_2 (5 mL) and added to the polypropylene fritted syringe with resin. The reaction slurry was shaken at ambient temperature for 16 h, followed by washing with CH_2Cl_2 (5 × 5 mL). Subsequent cleavage from the resin and UHPLC-MS analysis confirmed the presence of desired product **10**. (ESI+ 373, 469 (trifluoroacetate)) Loading after this step (0.40 mmol/g) was determined as follows: the sample of resin **10** (~30 mg) was washed with CH_2Cl_2 (5 × 3 mL) and MeOH (3 × 3 mL), dried under a stream of nitrogen and divided into two portions (2 × 12 mg). Both samples were treated with CH_2Cl_2/TFA (1:1, 1 mL, v/v) for 1 h, after which the cleavage cocktail was evaporated under a stream of nitrogen. Cleaved compounds were dissolved in CH_3CN/H_2O (1:1, 1 mL, v/v), diluted four times, and analyzed by ultra-high performance liquid chromatography coupled with mass spectrometry and ultraviolet detection (UHPLC/MS/UV). Loading of the resin was calculated with the use of an external standard (Fmoc-Ala-OH, 0.5 mg/mL).

4.3.11. Procedure for tosylation

Resin **10** (500 mg) was swollen in CH_2Cl_2 (5 mL) for 30 min and then washed with CH_2Cl_2 (3 × 5 mL). Tosyl chloride (285 mg, 1.5 mmol), Et_3N (209 μL, 1.5 mmol) and DMAP (61 mg, 0.5 mmol) were dissolved in dry CH_2Cl_2 (5 mL) and added to the propylene fritted syringe with resin **10**. The reaction slurry was shaken at ambient temperature for 16 h, followed by washing with DMF (5 × 5 mL) and CH_2Cl_2 (3 × 5 mL). Subsequent cleavage from the resin and UHPLC-MS analysis confirmed the presence of desired product **11**. (ESI+ 527).

*4.3.12. Procedure for nucleophilic substitution with **7***

Resin **11** (250 mg) was swollen in CH_2Cl_2 (5 mL) for 30 min, washed with CH_2Cl_2 (3 × 5 mL) and added to the ace-pressure tube with solution of purine ligand **7** (86 mg, 0.15 mmol) and DIPEA (247 μL, 1.5 mmol) in DMF (2.5 mL). The reaction slurry was stirred at 70 °C for 16 h, followed by washing with DMF (5 × 5 mL) and CH_2Cl_2 (3 × 5 mL). Subsequent cleavage from the resin and UHPLC-MS analysis confirmed the presence of desired product **12**. (ESI- 828).

4.3.13. Procedure for deprotection of Fmoc on resin

Resin (250 mg) was swollen in CH_2Cl_2 (3 mL) for 30 min and then washed with DMF (3 × 3 mL). The freshly prepared solution of CH_2Cl_2/DBU (1:1, 3 mL, v/v) was added to polypropylene fritted syringe with the resin. The reaction slurry was shaken at ambient temperature for 10 min, followed by washing with CH_2Cl_2 (3 × 3 mL), THF (3 × 3 mL) and CH_2Cl_2 (3 × 3 mL). Resin was used directly into the next step without further analysis.

*4.3.14. Procedure for acylation with **8** and final cleavage from the resin*

Resin **12** (250 mg) was swollen in CH_2Cl_2 (3 mL) for 30 min and then washed with CH_2Cl_2 (3 × 3 mL). Pom-Gly **8** (165 mg, 0.5 mmol) and HOBt (72 mg, 0.5 mmol) were dissolved in DMF (2.5 mL), followed by addition of DIC (80 μL, 0.5 mmol). The mixture was added to the propylene fritted syringe with resin **12** and the reaction slurry was shaken at ambient temperature for 16 h, followed by washing with DMF (5 × 5 mL) and CH_2Cl_2 (3 × 5 mL). Subsequent cleavage from the resin and UHPLC-MS analysis confirmed the presence of desired product **13**.

4.3.15. Final cleavage from the resin prior to HPLC purification

The corresponding resin (250 mg) was swollen in CH_2Cl_2 (3 mL). Solution of CH_2Cl_2/TFA (1:1, 6 mL, v/v) was added to polypropylene fritted syringe with resin. The reaction slurry was shaken at ambient temperature for 2 h and then washed with CH_2Cl_2/TFA (1:1, 3 × 3 mL, v/v) and CH_2Cl_2 (3 × 3 mL). The cleavage cocktail with combined washes were evaporated under a stream of nitrogen, the crude product was dissolved in CH_3CN/H_2O (3:1, 5 mL, v/v) and purified by RP-HPLC to afford final compound **13** as yellowish oil (2 mg, 2% overall yield calculated from **10**).

4.4. Molecular modeling

Molecular docking of **BPA311** was performed with the FLT3 DFG-in model published previously [21] and with crystal structure of phosphorylated CDK9/cyclin T (PDB: 7NWK) co-crystalised with imidazo[4,5-*b*]pyridine ATP-competitive inhibitor.

Next, we prepared 3D structures of FLT3-CRBN and CDK9-CRBN based on a previously published crystal complexes of BRD4-CRBN and BTK-CRBN [36] constructed by molecular modelling in PRosettaC [37]. BTK was replaced by FLT3 or CDK9 based on structural alignment and homologous complexes with increasing distance between kinase domain and CRBN were obtained. These complexes were used as targets for docking of the PROTAC to find the optimal distance between the kinase and CRBN proteins in which both heads of the PROTAC were oriented properly with same interactions as in docking into protein monomers. The 3D structures of all compounds were obtained and their energy was minimized by molecular mechanics with Avogadro 1.90.0, a software for the characterization of chemical structures. Polar hydrogens were added to ligands and proteins with the AutoDock Tools program [38] and docking studies were performed using AutoDock Vina 1.05 [39]. Figures were generated using Pymol ver. 2.0.4 (Schrödinger, LLC).

4.5. Kinase-selectivity profiling

Protein kinase selectivity of **BPA311** and PROTAC **13** was evaluated at a single concentration (100 nM) by screening against 46 enzymes at Eurofins Discovery.

4.6. Cell cultures and viability assay

Human cell lines were obtained from the German Collection of Microorganisms (MOLM-13, RS4-11, Kasumi-1, THP-1, U937), European Collection of Authenticated Cell Cultures (K562), Cell lines service (MV4-11) or were generously gifted by G. E. Winter (CRBN-deficient MV4-11) and were cultivated according to the provider's instructions. Briefly, cells were maintained in RPMI-1640 medium (or DMEM for K562) supplemented with 10% fetal bovine serum, penicillin (100 U/mL), and streptomycin (0.1 mg/mL) at 37 °C in 5% CO_2.

For the viability assays, cells were treated in triplicate with six different doses of each compound for 72 h. After treatments, resazurin (Sigma Aldrich) solution was added for 4 h, and fluorescence of resorufin corresponding to live cells was measured at 544 nm/590 nm (excitation/emission) using a Fluoroskan Ascent microplate reader (Labsystems). The GI_{50} value, the drug concentration lethal to 50% of the cells, was calculated from the dose response curves that resulted from the assays.

4.7. Immunoblotting

Cell lysates were prepared, and then proteins were separated on SDS-polyacrylamide gels and electroblotted onto nitrocellulose membranes. After blocking, overnight incubation with specific primary antibodies, and incubation with peroxidase-conjugated secondary antibodies, peroxidase activity was detected with Super-Signal West Pico reagents (Thermo Scientific) using a CCD camera LAS-4000 (Fujifilm). The specific antibodies were purchased from Cell signaling (anti-FLT3, clone 8F2; anti-phospho-FLT3 Y589/591, clone 30D4; anti-STAT5; anti-phospho-STAT5 Y694; anti-ERK1/2; anti-phospho-ERK1/2 T202/Y204; anti-PARP-1, clone 46D11; peroxidase-conjugated secondary antibodies), Santa Cruz Biotechnology (anti-CDK9, clone D-7), DAKO (anti-ubiquitin), Atlas Antibodies (anti-CRBN) or were generously gifted by Dr. B. Vojtěšek (anti-PCNA, clone PC-10).

4.8. Flow cytometry

Asynchronously growing cells were seeded and, after a preincubation period, treated with tested compounds for 24 h. After the staining with propidium iodide, DNA content was analyzed by flow cytometry using a 488 nm laser (BD FACS Verse with software BD FACSuiteTM, version 1.0.6.). Cell cycle distribution was analyzed using ModFit LT (Verity Software House).

4.9. Caspase 3/7 assay

Cell lysates were incubated with 100 μM Ac-DEVD-AMC (Enzo Life Sciences) as a substrate of caspases 3 and 7 in the assay buffer (25 mM PIPES, 2 mM EGTA, 2 mM $MgCl_2$, 5 mM DTT, pH 7.3). The fluorescence of the product was measured using a Fluoroskan Ascent microplate reader (Labsystems) at 355/460 nm (ex/em).

Alternatively, cellular caspase-3/7 activity was measured according to a previously published procedure [40]. Cells were cultivated in a 96-well plate and treated with increasing concentrations of compounds for 16 h. After incubation, 3 × caspase-3/7 assay buffer (150 mM HEPES pH 7.4, 450 mM NaCl, 150 mM KCl, 30 mM MgCl2, 1.2 mM EGTA, 1.5% Nonidet P40, 0.3% CHAPS, 30% sucrose, 30 mM DTT, 3 mM PMSF) containing 150 μM peptide substrate Ac-DEVD-AMC (Enzo Life Sciences) was added. After 4 h incubation, the caspase-3/7 activity was measured using a Fluoroskan Ascent microplate reader (Labsystems) at 346 nm/442 nm (ex/em).

4.10. RNA isolation and qPCR

Total RNA was isolated using RNeasy plus mini kit (QIAGEN) according to the manufacture's instruction, and RNA concentration and purity was measured by DeNovix DS-11 spectrophotometer. RNA was transcribed into first-strand cDNA using SensiFast cDNA Synthesis Kit (Bioline). Quantitative RT-PCR was carried out on CFX96 Real-Time PCR Detection System (Biorad) with a SensiFAST SYBR No-Rox Kit (Bioline). The suitable primers were designed using Primer-BLAST [41] and synthesized by Generi Biotech. Primary data were analyzed using Bio-rad CFX Manager. Relative gene expression levels were deter-mined using delta delta Ct method [42]. Expressions were normalized per GADPH and RPL13A genes which were determined as the most stable by RefFinder Software [43].

Used primers: BCL-2 (F: ATGTGTGTGGAGAGCGTCA; R: ACAGCCAGGAGAAATCAAACAG); FLT3 (F: GGAATGGGTGCTTTGCGATT; R: CAGCACCTTATGTCCGTCCC); GAPDH (F: TCCAAAATCAAGTGGGGCGA; R: TGGTTCACACCCATGACGAA); HOXA9 (F: CCTGACTGACTATGCTTGTGGT; R: ACTCTTTCTCCAGTTCCAGGG); MEIS-1 (F: CGTCACAAAAAGCGTGGCAT; R: ATGGTGAGTCCCGTGTCTTG); MCL-1 (F: AGTTGTACCGGCAGTCG; R: TTTGATGTCCAGTTTCCGAAG); MYB (F: TCTCCAGTCATGTTCCATACCC; R: TGTGTGGTTCTGTGTTGGTAGC); MYC (F: TACAACACCCGAGCAAGGAC; R: AGCTAACGTTGAGGGGCATC); RPL13A (F: CGACAAGAAAAAGCGGATGG; R: TTCTCTTTCCTCTTCTCCTCC).

Author contributions

E.Ř., M.P. and M.K. performed cellular experiments, S.K. and M.S. prepared and analyzed compounds, M.P. and V.K. analyzed binding modes, E.Ř., S.K., M.S. and V.K. designed the study and wrote the manuscript.

Declaration of competing interest

The authors declare that they have no known competing financial interests or personal relationships that could have appeared to influence the work reported in this paper.

Data availability

Data will be made available on request.

Acknowledgements

Authors thank Georg E. Winter for providing CRBN-deficient MV4-11 cells and Sophie Day-Riley for grammar proofreading corrections. The work was supported by the European Union - Next Generation EU (The project National Institute for Cancer Research, Programme EXCELES, ID No. LX22NPO5102), Czech Science Foundation (19-09086S) and Palacký University Olomouc (IGA_2022_007).

Appendix A. Supplementary data

Supplementary data to this article can be found online at https://doi.org/10.1016/j.ejmech.2022.114792.

References

[1] H. Döhner, D.J. Weisdorf, C.D. Bloomfield, Acute myeloid leukemia, N. Engl. J. Med. 373 (2015) 1136–1152, https://doi.org/10.1056/NEJMra1406184.
[2] R.M. Shallis, R. Wang, A. Davidoff, X. Ma, A.M. Zeidan, Epidemiology of acute myeloid leukemia: recent progress and enduring, Blood Rev. 36 (2019) 70–87, https://doi.org/10.1016/j.blre.2019.04.005.
[3] J.U. Kazi, L. Rönnstrand, FMS-Like tyrosine kinase 3/FLT3: from basic science to clinical implications, Physiol. Rev. 99 (2019) 1433–1466, https://doi.org/10.1152/physrev.00029.2018.
[4] M. Levis, Midostaurin approved for FLT3-mutated AML, Blood 129 (2017) 3403–3406, https://doi.org/10.1182/blood-2017-05-782292.
[5] S. Dhillon, Gilteritinib: first global approval, Drugs 79 (2019) 331–339, https://doi.org/10.1007/s40265-019-1062-3.
[6] K. Kidoguch, M. Shibusawa, T. Tanimoto, A critical appraisal of Japan's new drug approval process: a case study of FLT3-ITD inhibitor quizartinib, Invest. N. Drugs 39 (2021) 1457–1459, https://doi.org/10.1007/s10637-021-01151-0.
[7] M. Wu, C. Li, X. Zhu, FLT3 inhibitors in acute myeloid leukemia, J. Hematol. Oncol. 11 (2018) 133, https://doi.org/10.1186/s13045-018-0675-4.
[8] S.S.Y. Lam, A.Y.H. Leung, Overcoming resistance to FLT3 inhibitors in the treatment of FLT3-mutated AML, Int. J. Mol. Sci. 21 (2020) 1537, https://doi.org/10.3390/ijms21041537.
[9] K.M. Sakamoto, K.B. Kim, A. Kumagai, F. Mercurio, C.M. Crews, R.J. Deshaies, Protacs: chimeric molecules that target proteins to the Skp1-Cullin-F box complex for ubiquitination and degradation, Proc. Natl. Acad. Sci. USA 98 (2001) 8554–8559, https://doi.org/10.1073/pnas.141230798.
[10] S.J. Hughes, A. Testa, N. Thompson, I. Churcher, The rise and rise of protein degradation: opportunities and challenges ahead, Drug Discov. Today 26 (2021) 2889–2897, https://doi.org/10.1016/j.drudis.2021.08.006.
[11] H.T. Huang, D. Dobrovolsky, J. Paulk, G. Yang, E.L. Weisberg, Z.M. Doctor, D. L. Buckley, J.H. Cho, E. Ko, J. Jang, K. Shi, H.G. Choi, J.D. Griffin, Y. Li, S.P. Treon, E.S. Fischer, J.E. Bradner, L. Tan, N.S. Gray, A chemoproteomic approach to query the degradable kinome using a multi-kinase degrader, Cell Chem. Biol. 25 (2018) 88–99, https://doi.org/10.1016/j.chembiol.2017.10.005, e6.
[12] G.M. Burslem, J. Song, X. Chen, J. Hines, C.M. Crews, Enhancing antiproliferative activity and selectivity of a FLT-3 inhibitor by proteolysis targeting chimera conversion, J. Am. Chem. Soc. 140 (2018) 16428–16432, https://doi.org/10.1021/jacs.8b10320.
[13] S. Cao, L. Ma, Y. Liu, M. Wei, Y. Yao, C. Li, R. Wang, N. Liu, Z. Dong, X. Li, M. Li, X. Wang, C. Yang, G. Yang, Proteolysis-targeting chimera (PROTAC) modification of dovitinib enhances the antiproliferative effect against FLT3-ITD-positive acute myeloid leukemia cells, J. Med. Chem. 64 (2021) 16497–16511, https://doi.org/10.1021/acs.jmedchem.1c00996.
[14] Y. Chen, X. Yuan, M. Tang, M. Shi, T. Yang, K. Liu, D. Deng, L. Chen, Degrading FLT3-ITD protein by proteolysis targeting chimera (PROTAC), Bioorg. Chem. 119 (2022), 105508, https://doi.org/10.1016/j.bioorg.2021.105508.
[15] S. Boffo, A. Damato, L. Alfano, A. Giordano, CDK9 inhibitors in acute myeloid leukemia, J. Exp. Clin. Cancer Res. 37 (2018) 36, https://doi.org/10.1186/s13046-018-0704-8.
[16] X. Han, N. Song, A. Saidahmatov, P. Wang, Y. Wang, X. Hu, W. Kan, W. Zhu, L. Gao, M. Zeng, Y. Wang, C. Li, J. Li, H. Liu, Y. Zhou, J. Wang, Rational design and development of novel CDK9 inhibitors for the treatment of acute myeloid leukemia, J. Med. Chem. 64 (2021) 14647–14663, https://doi.org/10.1021/acs.jmedchem.1c01148.
[17] T. Yin, M.J. Lallena, E.L. Kreklau, K.R. Fales, S. Carballares, R. Torrres, G. N. Wishart, R.T. Ajamie, D.M. Cronier, P.W. Iversen, T.I. Meier, R.T. Foreman, D. Zeckner, S.E. Sissons, B.W. Halstead, A.B. Lin, G.P. Donoho, Y. Qian, S. Li, S. Wu, A. Aggarwal, X.S. Ye, J.J. Starling, R.B. Gaynor, A. de Dios, J. Du, A novel CDK9 inhibitor shows potent antitumor efficacy in preclinical hematologic tumor models, Mol. Cancer Therapeut. 13 (2014) 1442–1456, https://doi.org/10.1158/1535-7163.MCT-13-0849.
[18] A.T. Anshabo, L. Bantie, S. Diab, J. Lenjisa, A. Kebede, Y. Long, G. Heinemann, J. Karanjia, B. Noll, S.K.C. Basnet, M. Li, R. Milne, H. Albrecht, S. Wang, An orally bioavailable and highly efficacious inhibitor of CDK9/FLT3 for the treatment of acute myeloid leukemia, Cancers 14 (2022) 1113, https://doi.org/10.3390/cancers14051113.
[19] D.C. Phillips, S. Jin, G.P. Gregory, Q. Zhang, J. Xue, X. Zhao, J. Chen, Y. Tong, H. Zhang, M. Smith, S.K. Tahir, R.F. Clark, T.D. Penning, J.R. Devlin, J. Shortt, E. D. Hsi, D.H. Albert, M. Konopleva, R.W. Johnstone, J.D. Leverson, A.J. Souers, A novel CDK9 inhibitor increases the efficacy of venetoclax (ABT-199) in multiple models of hematologic malignancies, Leukemia 34 (2020) 1646–1657, https://doi.org/10.1038/s41375-019-0652-0.
[20] D.A. Luedtke, Y. Su, J. Ma, X. Li, S.A. Buck, H. Edwards, L. Polin, J. Kushner, S. H. Dzinic, K. White, H. Lin, J.W. Taub, Y. Ge, Inhibition of CDK9 by voruciclib synergistically enhances cell death induced by the Bcl-2 selective inhibitor venetoclax in preclinical models of acute myeloid leukemia, Signal Transduct. Targeted Ther. 5 (2020) 17, https://doi.org/10.1038/s41392-020-0112-3.
[21] T. Gucký, E. Řezníčková, T. Radošová Muchová, R. Jorda, Z. Klejová, V. Malínková, K. Berka, V. Bazgier, H. Ajani, M. Lepšík, V. Divoký, V. Kryštof, Discovery of N 2-(4-Amino-cyclohexyl)-9-cyclopentyl- N 6-(4-morpholin-4-ylmethyl-phenyl)- 9H-purine-2,6-diamine as a potent FLT3 kinase inhibitor for acute myeloid leukemia with FLT3 mutations, J. Med. Chem. 61 (2018) 3855–3869, https://doi.org/10.1021/acs.jmedchem.7b01529.
[22] T. Gucký, R. Jorda, M. Zatloukal, V. Bazgier, K. Berka, E. Řezníčková, T. Béres, M. Strnad, V. Kryštof, A novel series of highly potent 2,6,9-trisubstituted purine cyclin-dependent kinase inhibitors, J. Med. Chem. 56 (2013) 6234–6247, https://doi.org/10.1021/jm4006884.
[23] R. Jorda, L. Havlíček, A. Šturc, D. Tušková, L. Daumová, M. Alam, J. Škerlová, M. Nekardová, M. Peřina, T. Pospíšil, J. Široká, L. Urbánek, P. Pachl, P. Řezáčová, M. Strnad, P. Klener, V. Kryštof, 3,5,7-Substituted pyrazolo[4,3-d]pyrimidine inhibitors of cyclin-dependent kinases and their evaluation in lymphoma models, J. Med. Chem. 62 (2019) 4606–4623, https://doi.org/10.1021/acs.jmedchem.9b00189.
[24] D. Dalgarno, T. Stehle, S. Narula, P. Schelling, M.R. van Schravendijk, S. Adams, L. Andrade, J. Keats, M. Ram, L. Jin, T. Grossman, I. MacNeil, C. Metcalf 3rd, W. Shakespeare, Y. Wang, T. Keenan, R. Sundaramoorthi, R. Bohacek, M. Weigele, T. Sawyer, Structural basis of Src tyrosine kinase inhibition with a new class of potent and selective trisubstituted purine-based compounds, Chem. Biol. Drug Des. 67 (2006) 46–57, https://doi.org/10.1111/j.1747-0285.2005.00316.x.
[25] D.P. Bondeson, B.E. Smith, G.M. Burslem, A.D. Buhimschi, J. Hines, S. Jaime-Figueroa, J. Wang, B.D. Hamman, A. Ishchenko, C.M. Crews, Lessons in PROTAC design from selective degradation with a promiscuous warhead, Cell Chem. Biol. 25 (2018) 78–87, https://doi.org/10.1016/j.chembiol.2017.09.010, e5.
[26] B.E. Smith, S.L. Wang, S. Jaime-Figueroa, A. Harbin, J. Wang, B.D. Hamman, C. M. Crews, Differential PROTAC substrate specificity dictated by orientation of recruited E3 ligase, Nat. Commun. 10 (2019) 131, https://doi.org/10.1038/s41467-018-08027-7.
[27] S. Krajcovicova, R. Jorda, D. Hendrychova, V. Krystof, M. Soural, Solid-phase synthesis for thalidomide-based proteolysis-targeting chimeras (PROTAC), Chem. Commun. 55 (2019) 929–932, https://doi.org/10.1039/c8cc08716d.
[28] C.M. Olson, B. Jiang, M.A. Erb, Y. Liang, Z.M. Doctor, Z. Zhang, T. Zhang, N. Kwiatkowski, M. Boukhali, J.L. Green, W. Haas, T. Nomanbhoy, E.S. Fischer, R. A. Young, J.E. Bradner, G.E. Winter, N.S. Gray, Pharmacological perturbation of CDK9 using selective CDK9 inhibition or degradation, Nat. Chem. Biol. 14 (2018) 163–170, https://doi.org/10.1038/nchembio.2538.
[29] S. Krajčovičová, T. Gucký, D. Hendrychová, V. Kryštof, M. Soural, A stepwise approach for the synthesis of folic acid conjugates with protein kinase inhibitors, J. Org. Chem. 82 (2017) 13530–13541, https://doi.org/10.1021/acs.joc.7b02650.
[30] S. Krajčovičová, J. Hlaváč, K. Vychodilová, Polymer-supported synthesis of N-substituted anthranilates as the building blocks for preparation of N-arylated 3-hydroxyquinolin-4(1H)-ones, RSC Adv. 11 (2021) 9362–9365, https://doi.org/10.1039/d1ra01308d.
[31] M. Brand, B. Jiang, S. Bauer, K.A. Donovan, Y. Liang, E.S. Wang, R.P. Nowak, J. C. Yuan, T. Zhang, N. Kwiatkowski, C.A. Müller, E.S. Fischer, N.S. Gray, G. E. Winter, Homolog-selective degradation as a strategy to probe the function of CDK6 in AML, Cell Chem. Biol. 26 (2019) 300–306, https://doi.org/10.1016/j.chembiol.2018.11.006, e9.
[32] D.E. Schmidt-Arras, A. Böhmer, B. Markova, C. Choudhary, H. Serve, F.D. Böhmer, Tyrosine phosphorylation regulates maturation of receptor tyrosine kinases, Mol. Cell Biol. 25 (2005) 3690–3703, https://doi.org/10.1128/MCB.25.9.3690-3703.2005.
[33] K. Reiter, H. Polzer, C. Krupka, A. Maiser, B. Vick, M. Rothenberg-Thurley, K. H. Metzeler, D. Dörfel, H.R. Salih, G. Jung, E. Nößner, I. Jeremias, W. Hiddemann, H. Leonhardt, K. Spiekermann, M. Subklewe, P.A. Greif, Tyrosine kinase inhibition increases the cell surface localization of FLT3-ITD and enhances FLT3-directed immunotherapy of acute myeloid leukemia, Leukemia 32 (2018) 313–322, https://doi.org/10.1038/leu.2017.257.
[34] E. Weisberg, A. Ray, E. Nelson, S. Adamia, R. Barrett, M. Sattler, C. Zhang, J. F. Daley, D. Frank, E. Fox, J.D. Griffin, Reversible resistance induced by FLT3 inhibition: a novel resistance mechanism in mutant FLT3-expressing cells, PLoS One 6 (2011), e25351, https://doi.org/10.1371/journal.pone.0025351.
[35] C. Larrue, E. Saland, H. Boutzen, F. Vergez, M. David, C. Joffre, M.A. Hospital, J. Tamburini, E. Delabesse, S. Manenti, J.E. Sarry, C. Récher, Proteasome inhibitors induce FLT3-ITD degradation through autophagy in AML cells, Blood 127 (2016) 882–892, https://doi.org/10.1182/blood-2015-05-646497.
[36] A. Zorba, C. Nguyen, Y. Xu, J. Starr, K. Borzilleri, J. Smith, H. Zhu, K.A. Farley, W. Ding, J. Schiemer, X. Feng, J.S. Chang, D.P. Uccello, J.A. Young, C.N. Garcia-Irrizary, L. Czabaniuk, B. Schuff, R. Oliver, J. Montgomery, M.M. Hayward, J. Coe, J. Chen, M. Niosi, S. Luthra, J.C. Shah, Delineating the role of cooperativity in the design of potent PROTACs for BTK, Proc. Natl. Acad. Sci. USA 31 (2018) E7285–E7292, https://doi.org/10.1073/pnas.1803662115.

[37] D. Zaidman, J. Prilusky, N. London, ProsettaC, Rosetta based modeling of PROTAC mediated ternary complexes, J. Chem. Inf. Model. 60 (2020) 4894–4903, https://doi.org/10.1021/acs.jcim.0c00589.
[38] G.M. Morris, R. Huey, W. Lindstrom, M.F. Sanner, R.K. Belew, D.S. Goodsell, A. J. Olson, AutoDock4 and AutoDockTools4: automated docking with selective receptor flexibility, J. Comput. Chem. 30 (2009) 2785–2791, https://doi.org/10.1002/jcc.21256.
[39] O. Trott, A.J. Olson, AutoDock Vina, Improving the speed and accuracy of docking with a new scoring function, efficient optimization, and multithreading, J. Comput. Chem. 31 (2009) 455–461, https://doi.org/10.1002/jcc.21334.
[40] R.A. Carrasco, N.B. Stamm, B.K.R. Patel, One-step cellular caspase-3/7 assay, Biotechniques 34 (2003) 1064–1067, https://doi.org/10.2144/03345dd02.
[41] J. Ye, G. Coulouris, I. Zaretskaya, I. Cutcutache, S. Rozen, T.L. Madden, Primer-Blast, A tool to design target-specific primers for polymerase chain reaction, BMC Bioinf. 13 (2012) 134, https://doi.org/10.1186/1471-2105-13-134.
[42] K.J. Livak, T.D. Schmittgen, Analysis of relative gene expression data using real-time quantitative PCR and the 2(-Delta Delta C(T)) Method, Methods 25 (2001) 402–408, https://doi.org/10.1006/meth.2001.1262.
[43] F. Xie, P. Xiao, D. Chen, L. Xu, B. Zhang, miRDeepFinder: a miRNA analysis tool for deep sequencing of plant small RNAs, Plant Mol. Biol. 80 (2012) 75–84, https://doi.org/10.1007/s11103-012-9885-2.